García Torregrosa, I.; Lobera González, MP.; Solis Díaz, C.; Atienzar Corvillo, PE.; Serra Alfaro, JM. (2011). Development of CO2 Protective Layers by Spray Pyrolysis for Ceramic Oxygen Transport Membranes. Advanced Materials. 1(4):618-625. doi:10.1002/aenm.201100169

García Torregrosa, I.; Lobera González, MP.; Solis Díaz, C.; Atienzar Corvillo, PE.; Serra Alfaro, JM. (2011). Development of CO2 Protective Layers by Spray Pyrolysis for Ceramic Oxygen Transport Membranes. Advanced Materials. 1(4):618-625. doi:10.1002/aenm.201100169

Development of CO_2 Protective Layers by Spray Pyrolysis for Ceramic Oxygen Transport Membranes

Iván García-Torregrosa, M. Pilar Lobera, Cecilia Solís, Pedro Atienzar, José M. Serra*

Instituto de Tecnología Química (Universidad Politécnica de Valencia - Consejo Superior de Investigaciones Científicas), Av. Naranjos s/n, E-46022 Valencia, Spain.

Abstract

Ceramic mixed ionic-electronic conducting (MIEC) membranes enable the very selective oxygen separation from air at high temperatures. Two major potential applications of oxygen-transport membranes are (1) oxygen production for oxyfuel power plants and (2) integration within high-temperature catalytic membrane reactors for methane or alkane upgrading by selective oxidative conversions. However, these applications involve the contact with carbon-bearing atmospheres and most of state-of-the-art highly-permeable MIEC membranes do not tolerate operation under CO_2-rich environments due to carbonation processes. The present contribution shows our first attempts in the development of ceria-based protective thin layers on monolithic LSCF membranes. Gd-doped ceria (CGO) deposition was carried out by air blast spray pyrolysis on mirror polished LSCF disc membranes. The layer thickness was maintained below 0.4 μm in order to prevent the formation of cracks during thermal cycling and minimize the limitations caused by the reduced oxygen permeability through the ceria layer. After optimization of the spraying process, smooth crack-free dense coatings were obtained with high crystallinity in the as-deposited state. The layers were characterized by XRD, SEM, AFM, DC-conductivity measurements, interferometry and optical microscopy. Oxygen separation was studied on coated LSCF using air as the feed and argon/CO_2 mixtures as the sweep gas in the temperature range 650-1000ºC. The protected membrane exhibited a higher stability than the un-coated LSCF membrane, although the nominal oxygen flux was slightly reduced at temperatures below 850ºC due to the limited ambipolar conductivity of doped ceria in the range of oxygen partial pressures that were investigated. Moreover, the protective layer (250 nm thickness) remained stable after the permeation testing.

Keywords: Spray pyrolysis, OTM, oxygen membrane, LSCF, doped ceria, CO_2, protection layer

Corresponding author: Dr. José M. Serra, jmserra@itq.upv.es, Tel. +34.963879448

1. Introduction

Oxygen transport membranes (OTM) based on mixed ionic–electronic conducting (MIEC) oxides allow the selective separation of oxygen at high temperature. These ceramic membranes can be integrated in oxyfuel power plants (to reduce NO_X emissions and facilitate CO_2 sequestration) or can be used in high temperature membrane reactors to carry out different reactions, e.g. natural gas conversion to syngas. The most promising materials are perovskites with the formula $ABO_{3-\delta}$[1]. Single phase materials such as $SrCo_{0.8}Fe_{0.2}O_{3-\delta}$ (SCF)[2], $Ba_{0.5}Sr_{0.5}Co_{0.8}Fe_{0.2}O_{3-\delta}$ (BSCF)[3], $La_{0.6}Sr_{0.4}Co_{0.2}Fe_{0.8}O_{3-\delta}$ (LSCF)[4] have shown high oxygen permeation fluxes even under oxidizing conditions at both membrane sides. LSCF is an interesting material for oxygen separation and is currently cited as a typical example of the mixed conducting ceramics with relatively-high oxygen permeability and acceptable thermo-structural stability. However, those perovskites are chemically unstable under large oxygen chemical potential gradients (e.g. air/methane) and in the presence of CO_2, SO_2 or H_2O, leading to degradation in performance with time [5-7]. A class of materials that offers high stability, tolerance against CO_2 and high ionic conductivity at high temperatures is doped ceria, e.g. $Ce_xGd_{1-x}O_{2-\delta}$ (CGO). However, these exhibit a significantly lower fluxes when compared to perovskite compounds[1] due to the lack of electronic conductivity under oxygen partial pressures above 10^{-5} atm. Moreover, CGO has long-term microstructural stability[8], reasonable chemical stability under low oxygen partial pressures[9], high catalytic activity and does not form undesirable secondary phases with typical perovskite cathode materials, such as $La_{1-x}Sr_xCoO_{3-\delta}$ and $La_{1-x}Sr_xCo_{1-y}Fe_yO_{3-\delta}$[1].

For potential industrial applications of LSCF membranes, several properties are crucial, i.e., high oxygen permeability, sufficient thermal and chemical stability, particularly in reducing gas atmospheres or atmospheres containing CO_2, as well as manufacturability and compatibility with other module materials. The use of a dense CGO thin film as protective layer could improve the chemical stability of the LSCF membranes. Concerning the physicochemical compatibility of CGO and LSCF, comparison of thermal expansion coefficients (TEC) is necessary to determine the mechanical compatibilities between the LSCF membrane and the CGO thin film. Although the TEC is 15 x 10^{-6} K^{-1} and 12 x 10^{-6} K^{-1} for LSCF and CGO respectively[10], the dense CGO thin film can tolerate a high TEC mismatch for certain layer thickness (below the critical thickness)[11], which could enable its use for this application.

CGO thin film layers can be prepared using diverse deposition techniques including RF-sputtering PVD[12], electron beam PVD[13, 14], dip coating[15], spin coating[16, 17], CVD[18], slip casting[4], screen printing[4, 14], plasma spraying[19], spray pyrolysis[20], etc. The preparation of gastight films typically by cost-effective conventional techniques requires subsequent thermal treatments at high temperatures and some degree of shrinkage in the substrate. CVD and other high-energy deposition techniques such as PVD and plasma spraying enable to a high density and gas tightness

to be achieved in the as-deposited films. The spray pyrolysis technique [21] is very attractive because it is scalable and potentially a low-cost process. Other advantages are the ability to control over the morphology and chemical composition by the choice of solvent, precursor concentrations, and droplet size and temperature deposition. In addition, direct high temperature deposition can avoid the appearance of cracks or uniformities due to internal stresses when layers are prepared at room temperature. Despite its potential advantages, the use of spray pyrolysis in the preparation of solid oxide fuel cells remains uncommon while there is no report on the preparation of oxygen transport membranes using this technique.

The present study aims to develop CGO protective coatings on monolithic LSCF membranes. The preparation procedure was tuned to achieve high-density thin films, which fully cover the LSCF membrane side exposed to CO_2-containing sweep. Firstly, the quality of the deposited films was assessed by XRD, AFM, SEM, optical microscopy and DC conductivity measurements. Furthermore, the permeation of the protected membrane will be systematically studied in the temperature range from 650 to 1000ºC, using Ar or a mixture Ar/CO_2 (85/15 vol.) as sweep gas. The effect of exposure to CO_2 at 750ºC for 48 h on the membrane permeation was also studied. Finally, post-mortem analyses (SEM and XRD) of the membranes was carried out to determine the possible evolution of the CGO top layer and LSCF membrane.

2. Experimental Procedure

2.1. CGO thin films preparation

2.1.1 Substrate preparation

Sapphire single crystal substrates (one side epi-polished) with *C-axis* orientation were purchased from ABCR. The original substrate (58.8 mm diameter x 0.332 mm thickness) was machined to dimensions of 10 x 10 x 0.33 mm. $La_{0.6}Sr_{0.4}Fe_{0.8}Co_{0.2}O_{3-\delta}$ (LSCF) substrates were prepared by uniaxial pressing followed by sintering at 1250ºC. The final membrane dimensions were 15 mm in diameter and ~ 0.8 mm thickness. After sintering the substrates were mechanically polished on both sides using a Struers Labosystem model Labopol-21 equipment until a surface roughness $R_a \leq 5$ nm was achieved. All substrates were cleaned and sonicated in acetone and isopropanol for 15 minutes prior layer deposition.

2.1.2 Precursors

For the preparation of $Ce_{0.9}Gd_{0.1}O_{2-\delta}$ (CGO) thin films, different precursors were investigated. In order to minimize the water content in the sprayed solution, a mixture of cerium acetylacetonate (acac) 0.045 mol l^{-1} (Sigma-Aldrich, 98% purity) and gadolinium acetylacetonate 0.005 mol l^{-1} (ABCR, 98% purity) were dissolved in N,N-

dimethylformamide (DMF, Sigma-Aldrich, 99% purity). According to the thermogravimetric analysis (TGA) performed, the physisorbed water content in the powder mixture is less than 12 % (150ºC) and the maximum mass loss (-63.5 %) is reached at 400 ºC, ascribed to the final acac decomposition and formation of the corresponding oxide. Different concentrations of the precursors, i.e. from 0.03 to 0.1 M, were tested and the most concentrated solutions required intensive stirring and heating. The most suited concentration of the precursors in DMF was 0.05 M and complete dissolution was achieved by heating at 80 ºC under stirring for two hours.

2.1.3 Spray pyrolysis set-up and procedure

The air blast spray pyrolysis conditions were kept constant for all the depositions shown in the present work. Depositions were made in an apparatus similar to that described elsewhere [22]. Nitrogen was used as carrier gas at different gas flow rates from 1 to 5 l min^{-1} and the best results were obtained using flows ranging from 2 to 4 l min^{-1}. A gas flow rate of 3 l min^{-1} at one bar pressure was set for all of the experiments carried out in this work. The spraying gun was a stainless steel Iwata High Performance C Plus with a nozzle diameter of 0.3 mm. Small variations of the distance (± 5 cm) between nozzle and substrate gave either rough surfaces with splashes or no deposition at all, which can be attributed to the Leidenfrost effect[23]. Spraying distance of 26 cm was found to be the most suitable for the sprayed solvent and temperature of the plate. A hot plate (Velp Scientifica) temperature ranging from 390 to 430 ºC was used in order to promote the ceria crystallization during the spraying process and fully crystalline thin films were achieved at nominal temperatures above 410 ºC. The hot plate temperature was heated at 430 ºC for all the substrates with a measured variation of ± 5ºC. The spraying frequency was one pulse every 5 seconds with pulse duration of 3 seconds. Typical deposition times were about one hour, which resulted in a film thickness of about 250 nm (deposition rate = 4.2 nm/min).

After thin film deposition, different heat treatments were performed in order to characterize the effect of the annealing temperature in the material. Films on sapphire single crystals were annealed at 600, 900 and 1000 ºC for 2 h (by heating up at 2 ºC/min and cooling down at 5 ºC/min) in air for structure characterization.

2.2. Characterization Techniques

The microstructure and the stability of the sintered layers were first observed by optical microscopy using a Nikon Microphot FX and then analyzed by Scanning electron microscopy (SEM) and energy dispersive spectroscopy (EDS) in a JEOL JSM6300 electron microscope, as well as by X-ray diffraction (XRD), using a Philips X'pert Pro equipped with X'celerator detector using monochromatic Cu Kα radiation. XRD patterns were recorded in the 2θ range from 10 to 90 º and analyzed using X'pert Highscore Plus software (PANalytical). For the grain size and roughness measurements of the thin films, atomic force microscopy (AFM) (Veeco Multimode) together with optical interferometry (Ambios Xi-100) were employed.

Electrical conductivity measurements were conducted by standard DC technique using in-plane four point configurations. Parallel silver electrodes were painted on the surface of a sprayed layer on sapphire substrate and silver wires were pasted in the electrodes. The constant current was supplied by a programmable current source (Keithley 2601) while the voltage drop was detected by a multimeter (Keithley 3706). In order to eliminate the thermal effect and to avoid non-ohmic responses, the voltage was measured with the current in both forward and reverse directions.

2.3. Oxygen permeation test

Oxygen permeation studies were carried out in a lab-scale membrane reactor [24]. The temperature was measured by a thermocouple close to the membrane. A PID controller maintained temperature variations within 2 ºC of the set point. The membrane consisted of a gastight ~ 0.8 mm thick LSCF disk (∅=15 mm) sintered with or without a protective CGO thin film. Sealing was done using gold gaskets. Oxygen was separated from a mixture of synthetic air while the sweep gas was either Ar or a mixture of Ar and CO_2. The permeate was analyzed by on-line gas chromatography using a micro-GC Varian CP-4900 equipped with Molsieve5A, Pora-Plot-Q glass capillary, and CP-Sil modules. All streams were individually mass flow controlled. Membrane leak-free conditions were ensured by continuously monitoring the nitrogen concentration in the product gas stream (just before and after switching to a pure O_2 feed). An acceptable sealing was achieved when the ratio between the oxygen flow leak and the oxygen flux was lower than 1%. The data reported here were achieved at steady state after one hour in the reaction stream. Each analysis was repeated three times to minimize the analysis error. The experimental analytical error was below 1 %.

3. Results and Discussion

3.1. Microstructural characterization of CGO thin films deposited on model substrates

Smooth, dense and homogeneous CGO thin films (thickness from 100 to 250 nm) were prepared on single crystal sapphire wafers and LSCF membranes after optimization of the mother solution and spraying process. Among others, cerium nitrate hexahydrate has been largely employed as precursor dissolved in different solvents and solvent mixtures [25-28], requiring the addition, in some cases, of pH stabilizing substances in order to obtain continuous and dense films. Ceria thin films deposited by ultrasonic spray pyrolysis were previously reported by M.F. Garcia-Sanchez et al.[25] using cerium acac as precursor dissolved in anhydrous methanol and crack-free films were only obtained when acetic acid was added to the solution. In our experiments the best results were obtained using cerium/gadolinium acac as precursors and DMF as solvent without any other additive. Spray pyrolysis using acac precursors in DMF was

an easy and novel method to obtain high quality CGO thin films. DMF is used due to the large solubility of the acac precursors and the high boiling point (153ºC). Indeed, quick evaporation of the solvent may lead to the formation of non adherent particles on the surface, resulting in a lower deposition yield[23]. Consequently, the higher vaporization point of DMF allows this phenomenon to be minimized with respect to other solvents such as ethanol (78ºC) or methanol (65ºC).

The as-prepared thin films deposited at 360 ºC became discontinuous and non-cohesive full of cracks. At temperatures below 400 ºC splashes of about 5 to 10 microns begin to appear and for temperatures above 410 ºC the thin films showed minimal splashes (due to excess material) and/or cracks on the surface, as can be seed from the optical microscope images shown in Figure 1. In contrast to previous reports, no additives were necessary to produce practically defect-free CGO thin films.

Figure 2 presents the XRD pattern of the as-deposited CGO film on sapphire substrate, where all the peaks can be assigned to the CGO fluorite structure together with the substrate reflections. The inset of Figure 2 shows the XRD patterns, from 26º to 35º, of an as-deposited film at 430 ºC, as well as of different films annealed at 600, 900 and 1000 ºC for 2 h. The patterns indicate that the CGO thin films are fully crystalline (fluorite structure) as-deposited at 430ºC. The higher intensity of the (200) reflection indicates a preferred orientation of the CGO films at all the temperatures, which increases at higher annealing temperatures. Although theoretically a (111) orientation is predicted, these (200) ceria textured films have been observed previously on different substrates deposited by different techniques [29-33]. As previously reported [29], it seems that there is a clear effect of the precursor / solvent on the texture of the ceria films. The evolution of the grain size (calculated using Scherrer equation) with annealing temperature can be observed from Figure 2b. Grain sizes are between 13 and 25 nm, in agreement with previously reported values [33, 34] whilst grain size growth takes place after treatment above 800 ºC, as also observed elsewhere [34].

According to the AFM and optical reflectometry data, the as-deposited CGO thin films are smooth and present a surface roughness of Ra~7 nm and grain sizes around 20 nm. AFM images shown in Figure 3 illustrate the coarsening effect of CGO thin films with increasing temperatures. The as-deposited sample (Figure 3a) and sample annealed at 600 ºC (Figure 3b) exhibit similar characteristics whereas the sample annealed at 900 ºC (Figure 3c) shows a significant increase in surface roughness of about 100% with typical values of Ra~15 nm.

3.2. Analysis of the protected LSCF membrane after permeation testing

Firstly, the possible thermal evolution of the LSCF substrate was studied. A mirror-polished LSFC membrane was treated in air at 1050 ºC for 12 hours and the surface remained unchanged as confirmed by SEM and AFM analysis. Therefore, the morphology changes in the CGO layer are assumed not to stem from substrate surface modifications. Figure 4 presents SEM images of (a) the top surface of the CGO layer

surface and (b) the polished cross-section corresponding to the protected LSCF membrane after permeation test, which included the treatment at several temperatures (max. 1000ºC) for several hours and a stability treatment in CO_2. The permeation test duration exceeded two weeks. From Figure 4, it can be inferred that the grain size is around 250 nm in average, reaching in some cases 350 nm in diameter. The layer thickness is ca. 250 nm and it is formed by a monolayer of grains, which are well-packed and bounded in the plane direction. Figure 4c shows an AFM image of CGO thin film surface after permeation experiment, analysis of which reveals a roughness of about 40 nm (Ra) and grain sizes in the range 250-350 nm. With respect to the samples annealed at lower temperatures (Figure 3, SCS substrates), a much greater increase in grain size and surface roughness is observed for membrane sample (max. exposure temperature 1000 ºC).

Figure 5 presents the XRD patterns (*log* scale) corresponding to the as-deposited CGO thin films on LSCF (a) at 430 ºC and (b) after permeation test at 1000 ºC. The most intense diffraction peaks of both patterns are assigned to the LSCF substrate (* symbols). In both cases the diffraction peaks corresponding to the fluorite structure are present (assigned Miller indexes indicated)while no other secondary phases are observed. From the higher intensity of the (200) peaks compared to (111) reflections, the same preferred orientation of the CGO films on LSCF can be inferred, as previously observed on sapphire single crystal substrates. By comparing both XRD patterns, crystallite growth (peak narrowing) can be observed in the tested sample (Figure 5b), while neither reaction products between CGO-LSCF nor significant cation interdiffusion can be detected within the limit of XRD. On the other hand, the CGO cell parameter remains constant in both samples (no appreciable changes in 2θ position are observed). In the pattern of the sample after permeation test, there is a new diffraction peak at 38.29º, assigned to the gold gasket used for membrane sealing.

3.3. Electrochemical study

Transport properties have been measured on the thin films deposited on SCS. Figure 6 shows the conductivity of a 250 nm CGO thin film (on SCS substrate) as a function of inverse temperature measured in air and in argon. The sample consists of a 250 nm thick layer on a sapphire substrate and was previously treated at 800 ºC in air. The conductivity results follow Arrhenius behaviour:

$$\sigma(T) = (A/T)\, exp(-E_a/kT) \qquad (1)$$

where E_a is the activation energy and k the Boltzmann constant.

Firstly, the conductivity is constant with the oxygen partial pressure (pO_2) and this behavior corresponds to the predominant ionic conduction. This is in agreement with the behavior of bulk polycrystalline CGO material in the measured range of pO_2. The obtained results are about 0.045 S/cm at 700 ºC, which agrees with reported data

for spray-pyrolyzed thin films (0.13-0.026 S/cm at 700 ºC depending on grain size [35, 36]). The E_a of 78.12 kJ/mol also agrees with reported values [35, 36].

3.4. Oxygen permeation test

Temperature dependence of oxygen permeation flux, $J(O_2)$, through LSCF membranes has been studied. Oxygen permeation was determined in the temperature range of 650-1000 ºC (Figure 7) for both the unprotected and the CGO-protected LSCF membrane (CGO layer thickness is 250 nm). The results indicate Arrhenius behaviour and the apparent activation energy (E_a) for oxygen transport changed at around 800 ºC, which is close to that reported elsewhere for BSCF membranes (775 ºC) and LSCF membranes (780 ºC), with similar membrane thicknesses [1]. This behaviour suggests that the rate-limiting step changes according to the temperature range investigated. Considering previous results, it can be inferred that the permeation at high temperatures is principally limited by bulk transport while the permeation rate at low temperatures is also affected by surface exchange processes.

The presence of the protective layer of CGO on the LSCF membrane had a negative effect in the permeation process, which was expected from the limited ambipolar conductivity of CGO in the studied pO_2 range. The $J(O_2)$ achieved with the protected membrane was lower than that obtained with the unprotected membrane in the whole temperature range, which was particularly evident at the lowest temperatures tested. At 650 ºC, the presence of the protective layer reduces the oxygen permeation flux by 60%, which is ascribed to the poor ambipolar conductivity and the lower surface exchange rate with respect to LSCF. In contrast, at higher temperatures the use of a protective layer only slightly affects the permeation process, which can be related to the higher ambipolar conductivity of the CGO layer in this temperature range, especially if small amounts of cobalt are present in the layer [37].

3.5. Effect of CO_2 presence in the sweep gas

The thermo-chemical and mechanical stability of the MIEC membranes are key issues for the use of these in practical applications. In the case of LSCF membranes, the poisoning effect of CO_2 is related to the fact that alkaline earth metals – included in the perovskite structure - tend to carbonate at the permeate side resulting in a drop of the oxygen permeation flux with time. However, a thin film of materials as CGO (with high stability and tolerance against CO_2) may act to protect the LSCF membrane.

Figure 8 shows the oxygen permeation flux through LSCF membranes as a function of the temperature when two different gas atmospheres were used in the permeate side: (1) argon and (2) 15 % CO_2 in argon. The experiments were carried out decreasing the temperature from 1000 ºC to 650 ºC. In the case of the unprotected LSCF membrane (Figure 8a), a decrease in the $J(O_2)$ was observed when the permeation test was carried out with 15% CO_2 in the sweep gas. This is ascribed to two possible interrelated processes: (i) slight carbonation of the membrane surface; and (ii)

competitive adsorption[38] between O_2 and CO_2, which may be important when surface exchange reaction is a major rate limiting step, i.e. at intermediate temperatures and/or for small membrane thicknesses. Nevertheless, the $J(O_2)$ was reduced to lesser extent at higher temperatures where the decomposition of the surface carbonates take place. The deposition of a CGO protective layer on the LSCF membrane allows the detrimental effect of the CO_2 presence on the $J(O_2)$ to be minimized (Figure 8b), since it prevents the carbonation reaction of strontium cations. However, the presence of CO_2 in the sweep gas slightly influenced the oxygen permeation of the protected membrane at low temperatures, which is attributed to the detrimental effect in the oxygen exchange process due to the competitive CO_2 adsorption[39].

In order to study the chemical stability in CO_2 gas atmosphere, the LSCF membranes were maintained in operation at 750 ºC for 48 h using 15 % CO_2 in argon as sweep. This experimental procedure was expected to lead to membrane surface degradation, which could be reversible or permanent. After that, the change of $J(O_2)$ with the temperature was studied. In a first step, the temperature was increased during the oxygen permeation tests (from 650 ºC to 1000 ºC), and then, in a consecutive step, these tests were repeated while the temperature was decreased (Figure 9). This experimental procedure was performed for the unprotected and protected LSCF membranes. The corresponding experimental $J(O_2)$ results are presented in Figure 10.

In the case of the unprotected LSCF membrane, carbonate species appeared to be formed in the membrane surface during the carbonation step, resulting in a hysteresis cycle of J_{O2} (Figure 10). This reversible degradation seems to be linked with the decomposition of the carbonates deposited on the membrane surface at higher temperatures; and the initial $J(O_2)$ can be fully recovered after treatment in Ar at 1000ºC. However, this degradation behavior is not observed for the protected LSCF membrane due to the negligible formation of carbonates on the outer CGO surface exposed to the CO_2 sweeping stream. These results demonstrate the effectiveness of the protective thin-layer against carbonation (reversible and irreversible), which is relevant to the industrial application of this kind of membranes. Additionally, these interesting results regarding the oxygen permeation should be considered together with the compatibility (thin CGO – bulk LSFC) and the stability of the CGO thin layer after treatments at 1000ºC for several days.

4. Conclusions and Outlook

CGO protective coatings have been developed on monolithic LSCF membranes by using spray pyrolysis. The final preparation procedure resulted in high-density films, which fully covered the LSCF membrane side, which was exposed to a CO_2-containing sweep. The quality of the deposited films has been confirmed by XRD, AFM, SEM, and optical microscopy. The films are crystalline fluorite structure already after deposition

at 430ºC. The evolution with temperature showed the grain growth in the layer and the thin film treated at 1000 ºC showed a monolayer of well-bounded grains. In-plane DC-conductivity measurements of CGO thin films deposited on sapphire single crystal confirmed the ionic conductivity values expected for Gd-doped ceria. Finally, the permeation of the protected/unprotected LSCF membranes has been systematically studied in the temperature range from 650 to 1000ºC and using Ar or a mixture Ar/CO_2 (85/15 vol.) as sweep gas. The main conclusions from the permeation study are:

- The presence of the thin CGO layer (250 nm) slightly decreases the oxygen flux and this effect is more visible at lower temperatures. This is ascribed to the limited ambipolar conductivity of CGO under high pO_2 environments.

- The effect of the CO_2 presence in the sweep gas is much more detrimental for the unprotected LSCF membranes.

- The oxygen permeation of the protected LSCF membrane remained stable after treatment at 750ºC in CO_2 for 48 hours while the permeation of the bare LSCF decreased substantially.

Post-mortem analysis of the membranes revealed that the CGO layer remained stable after the permeation test and there is not any reaction between CGO top layer and LSCF membrane within the limit of XRD and SEM. Long-term thermo-chemical and mechanical of the LSFC-CGO assembly should be addressed in future in planar or tubular membrane modules under realistic operating conditions.

Acknowledgements

Financial support by the Spanish Ministry for Science and Innovation (Project ENE2008-06302 and FPI Grant JAE-Pre 08-0058), EU through FP7 NASA-OTM Project (NMP3-SL-2009-228701), and the Helmholtz Association of German Research Centers through the Helmholtz Alliance MEM-BRAIN (Initiative and Networking Fund) is kindly acknowledged.

References

[1] J. Sunarso, S. Baumann, J. M. Serra, W. A. Meulenberg, S. Liu, Y. S. Lin, J. C. Diniz da Costa, *Journal of Membrane Science* **2008**, 320, 13.
[2] J. Vente, S. McIntosh, W. Haije, H. Bouwmeester, *Journal of Solid State Electrochemistry* **2006**, 10, 581.
[3] A. Leo, S. Smart, S. Liu, J. C. Diniz da Costa, *Journal of Membrane Science* **2011**, 368, 64.
[4] O. Büchler, J. M. Serra, W. A. Meulenberg, D. Sebold, H. P. Buchkremer, *Solid State Ionics* **2007**, 178, 91.
[5] M. Arnold, H. Wang, A. Feldhoff, *Journal of Membrane Science* **2007**, 293, 44.
[6] H. J. M. Bouwmeester, A. J. Burggraaf, A. J. Burggraaf, L. Cot, in *Membrane Science and Technology*, Vol. Volume 4, Elsevier, 1996, 435.
[7] V. V. Kharton, A. V. Kovalevsky, A. P. Viskup, A. L. Shaula, F. M. Figueiredo, E. N. Naumovich, F. M. B. Marques, *Solid State Ionics* **2003**, 160, 247.
[8] V. V. Kharton, A. A. Yaremchenko, E. N. Naumovich, F. M. B. Marques, *Journal of Solid State Electrochemistry* **2000**, 4, 243.
[9] V. V. Kharton, F. M. Figueiredo, L. Navarro, E. N. Naumovich, A. V. Kovalevsky, A. A. Yaremchenko, A. P. Viskup, A. Carneiro, F. M. B. Marques, J. R. Frade, *Journal of Materials Science* **2001**, 36, 1105.
[10] G. Corbel, S. Mestiri, P. Lacorre, *Solid State Sciences* **2005**, 7, 1216.
[11] P. V. Hendriksen, J. R. Høgsberg, A. M. Kjeldsen, B. F. Sørensen, H. G. Pedersen, *Failure Modes of Thin Supported Membranes*, John Wiley & Sons, Inc., 2008.
[12] E. Gourba, A. Ringuede, M. Cassir, A. Billard, J. Paiviasaari, J. Niinisto, M. Putkonen, L. Niinisto, *Ionics* **2003**, 9, 15.
[13] S. Uhlenbruck, N. Jordan, J. M. Serra, H. P. Buchkremer, D. Stöver, *Solid State Ionics* **2010**, 181, 447.
[14] S. Uhlenbruck, N. Jordan, D. Sebold, H. P. Buchkremer, V. A. C. Haanappel, D. Stöver, *Thin Solid Films* **2007**, 515, 4053.
[15] Y. L. Zhang, H. F. Gao, D. K. Peng, M. Y. Meng, X. Q. Liu, *Ceramics International* **2004**, 30, 1049.
[16] S. Q. Wang, M. Awano, K. Maeda, *Journal of the Ceramic Society of Japan* **2002**, 110, 780.
[17] M. Schulz, R. Kriegel, A. Kämpfer, *Journal of Membrane Science*, In Press, Corrected Proof.
[18] S. Jin, Y. Yang, J. E. Medvedeva, L. Wang, S. Li, N. Cortes, J. R. Ireland, A. W. Metz, J. Ni, M. C. Hersam, A. J. Freeman, T. J. Marks, *Chemistry of Materials* **2008**, 20, 220.
[19] R. Hui, Z. Wang, O. Kesler, L. Rose, J. Jankovic, S. Yick, R. Maric, D. Ghosh, *Journal of Power Sources* **2007**, 170, 308.
[20] D. Perednis, L. J. Gauckler, *Solid State Ionics* **2004**, 166, 229.
[21] G. L. Messing, S.-C. Zhang, G. V. Jayanthi, *Journal of the American Ceramic Society* **1993**, 76, 2707.
[22] D. Beckel, A. Dubach, A. Studart, L. Gauckler, *Journal of Electroceramics* **2006**, 16, 221.
[23] J. D. Bernardin, I. Mudawar, *Journal of Heat Transfer-Transactions of the Asme* **1999**, 121, 894.

[24] M. P. Lobera, S. Valero, J. M. Serra, S. Escolástico, E. Argente, V. Botti, *Chemical Engineering Science* **2011**, In Press.
[25] M. F. García-Sánchez, A. Ortiz, G. Santana, M. Bizarro, J. Peña, F. Cruz-Gandarilla, M. A. Aguilar-Frutis, J. C. Alonso, *Journal of the American Ceramic Society* **2010**, 93, 155.
[26] K. Konstantinov, I. Stambolova, P. Peshev, B. Darriet, S. Vassilev, *International Journal of Inorganic Materials* **2000**, 2, 277.
[27] N. L. Petrova, R. V. Todorovska, D. S. Todorovsky, *Solid State Ionics* **2006**, 177, 613.
[28] S. Wang, W. Wang, Q. Liu, M. Zhang, Y. Qian, *Solid State Ionics* **2000**, 133, 211.
[29] W. B. Carter, G. W. Book, T. A. Polley, D. W. Stollberg, J. M. Hampikian, *Thin Solid Films* **1999**, 347, 25.
[30] S. Gnanarajan, N. Savvides, *Thin Solid Films* **1999**, 350, 124.
[31] Y. J. Kim, Y. Gao, G. S. Herman, S. Thevuthasan, W. Jiang, D. E. McCready, S. A. Chambers, *Journal of Vacuum Science & Technology A: Vacuum, Surfaces, and Films* **1999**, 17, 926.
[32] S. H. Overbury, D. R. Huntley, D. R. Mullins, K. S. Ailey, P. V. Radulovic, "Surface studies of model supported catalysts: NO adsorption on Rh/CeO_2 (001)", 1997.
[33] J. L. M. Rupp, B. Scherrer, A. S. Harvey, L. J. Gauckler, *Advanced Functional Materials* **2009**, 19, n/a.
[34] T. Suzuki, I. Kosacki, H. U. Anderson, *Solid State Ionics* **2002**, 151, 111.
[35] G. Chiodelli, L. Malavasi, V. Massarotti, P. Mustarelli, E. Quartarone, *Solid State Ionics* **2005**, 176, 1505.
[36] J. L. M. Rupp, L. J. Gauckler, *Solid State Ionics* **2006**, 177, 2513.
[37] M. Balaguer, C. Solís, J. M. Serra, *Chemistry of Materials* **2011**, 23, 2333.
[38] A. Yan, B. Liu, Y. Dong, Z. Tian, D. Wang, M. Cheng, *Applied Catalysis B: Environmental* **2008**, 80, 24.
[39] V. B. Vert, J. M. Serra, *Journal of Power Sources* **2011**, 196, 4270.

FIGURE CAPTIONS

Figure 1. Optical microscope images of CGO thin films as-deposited at 430ºC on single crystal sapphire at 400X. (a) 100 nm CGO layer. (b) 250 nm CGO layer.

Figure 2. (a) XRD pattern of CGO thin films (250 nm thickness) deposited on single crystal sapphire by spray pyrolysis at 430º C (nominal substrate temperature). Inset shows a detail (26º-35º) of the evolution after heat treatment at different temperatures; and (b) Grain size evolution as a function of the annealing temperature.

Figure 3. AFM images of CGO thin films on single crystal sapphire (a) as-deposited; (b) after annealing at 600 ºC; (c) after annealing at 900 ºC.

Figure 4. (a) SEM top view; (b) corresponding SEM cross section and (c) AFM image of CGO sprayed pyrolysis deposited thin films on LSFC membrane after permeation experiment.

Figure 5. XRD patterns of CGO thin films (250 nm thickness) deposited on the LSCF membrane by spray pyrolysis at 430 ºC: (a) as deposited and (b) after permeation test at 1000 ºC. LSCF peaks are indicated by (*), CGO peaks by its Miller indexes and residual gold from gasket by (o).

Figure 6. Arrhenius plot for the total conductivity of the CGO layer deposited on a sapphire substrate recorded in dry argon and air. The CGO layer thickness is 250 nm and the averaged crystallite size is 100 nm.

Figure 7. Oxygen permeation flux through LSCF membranes as a function of temperature. Q_{Sweep}=65 ml min^{-1} (argon as sweep gas); Q_{Air}=60 ml min^{-1} (synthetic air, pO_2=0.21 atm).

Figure 8. Oxygen permeation flux through LSCF membranes as a function of temperature. Feed composition was O_2 (21 % v/v) in nitrogen Q_{Air}=60 ml min^{-1}; sweep gas was Ar or a mixture Ar/CO_2 (85/15 vol.); Q_{Sweep}=65 ml min^{-1}. (a) un-protected LSCF membrane; (b) CGO thin film on LSCF membrane.

Figure 9. Experimental procedure for the CO_2 stability.

Figure 10. Oxygen permeation flux through LSCF membranes as a function of temperature after 48 h in CO_2 gas atmosphere. Feed composition was synthetic air (pO_2=0.21 atm), argon was used as sweep gas. Q_{Sweep}=65 ml min^{-1}, Q_{Air}=60 ml min^{-1}. (a) un-protected LSCF membrane; (b) CGO thin film on LSCF membrane.

Figure 1

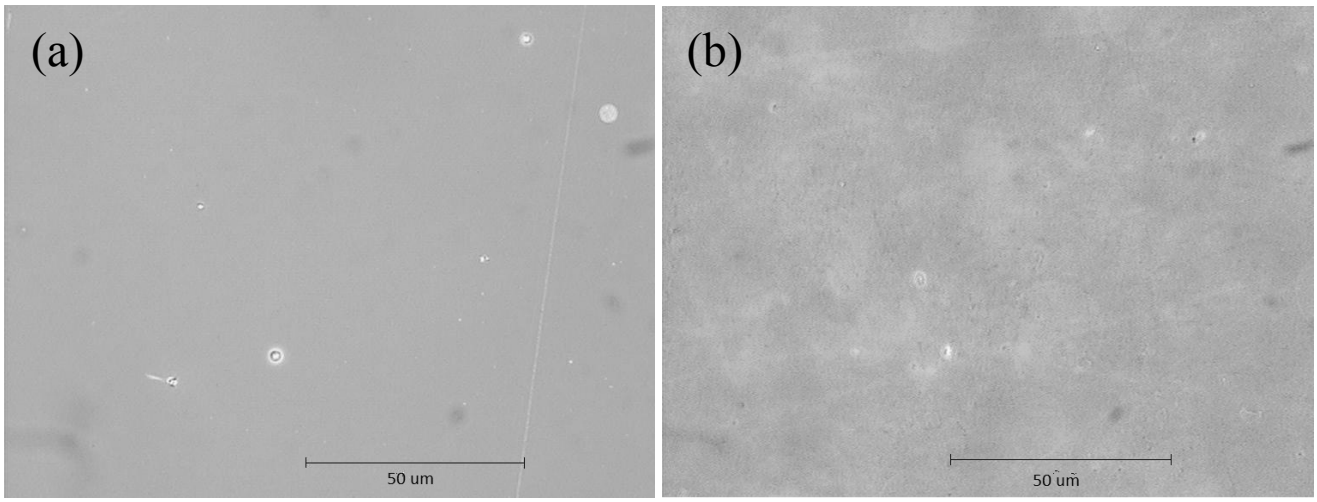

Figure 2

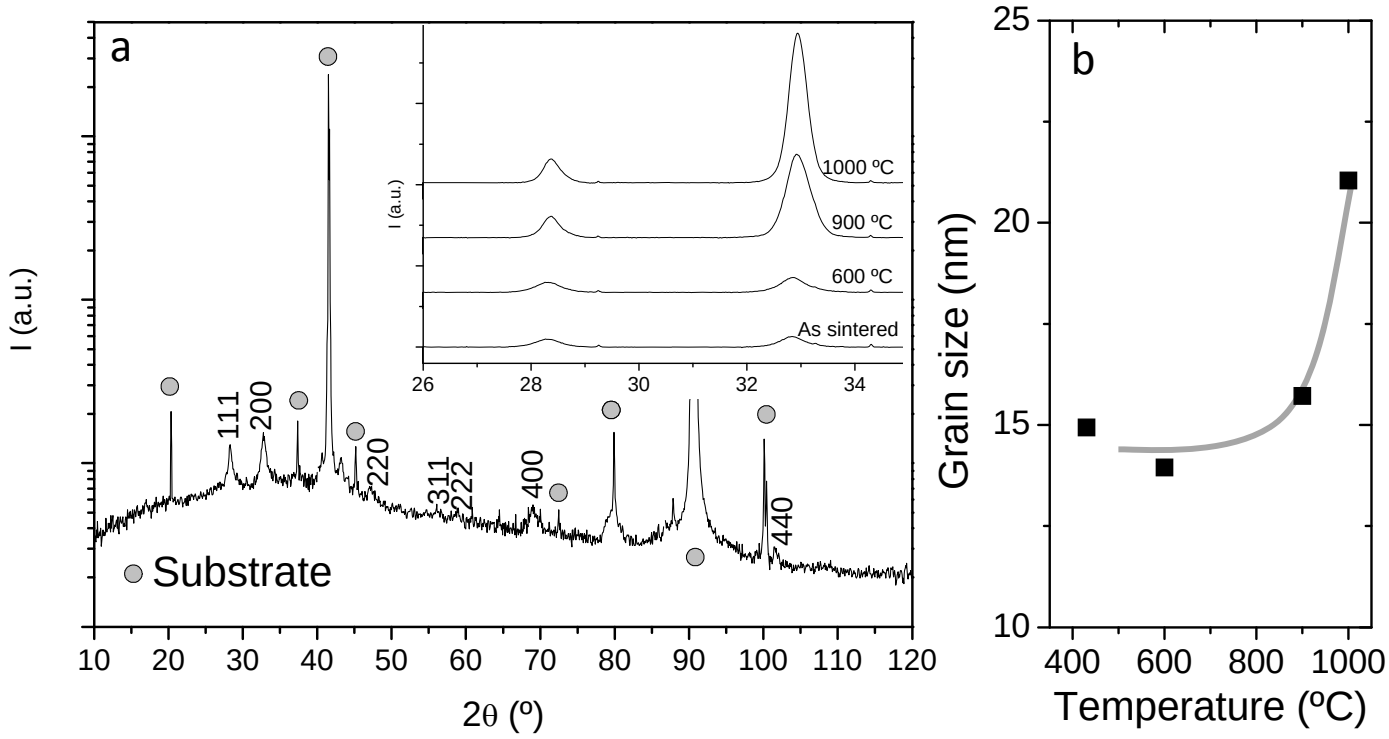
a
I (a.u.)
2θ (º)
Substrate
111
200
220
311
222
400
440
1000 ºC
900 ºC
600 ºC
As sintered
b
Grain size (nm)
Temperature (ºC)

Figure 3

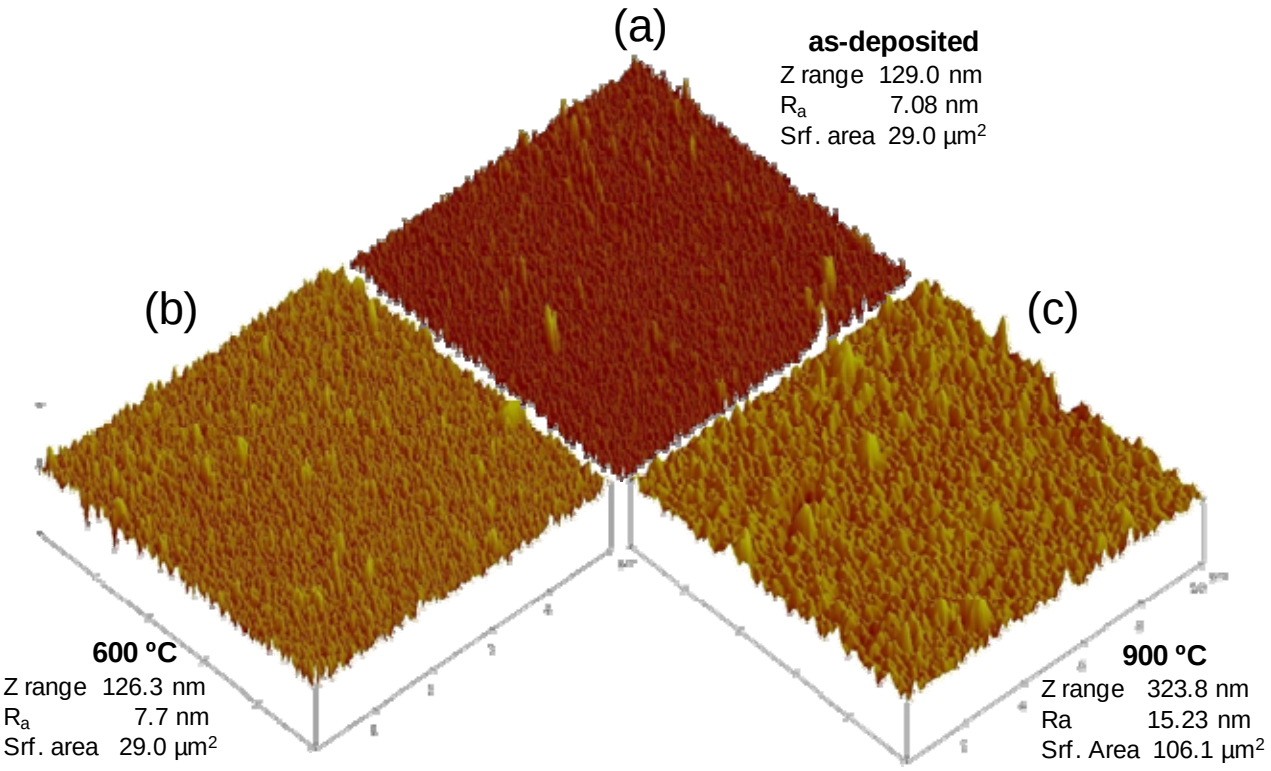
(a)
as-deposited
Z range 129.0 nm
R_a 7.08 nm
Srf. area 29.0 µm²
(b)
600 °C
Z range 126.3 nm
R_a 7.7 nm
Srf. area 29.0 µm²
(c)
900 °C
Z range 323.8 nm
Ra 15.23 nm
Srf. Area 106.1 µm²

Figure 4

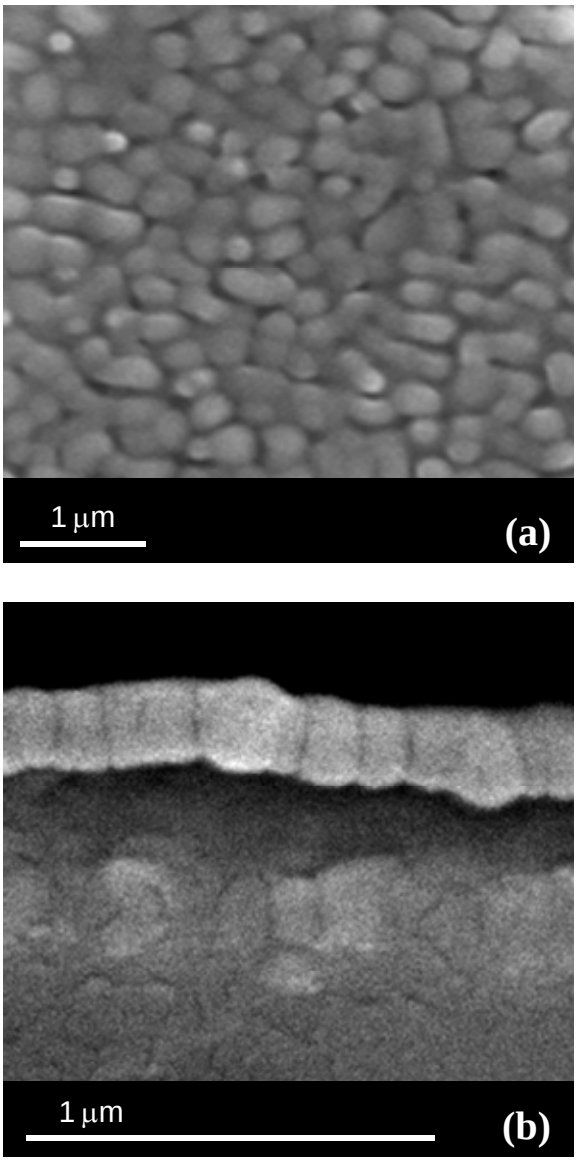
1 μm
(a)
1 μm
(b)
1000 ºC
Z range 543.96 nm
Ra 40.83 nm
Srf. area 127.28 um²
2
4
6
8
μm
(c)

Figure 5

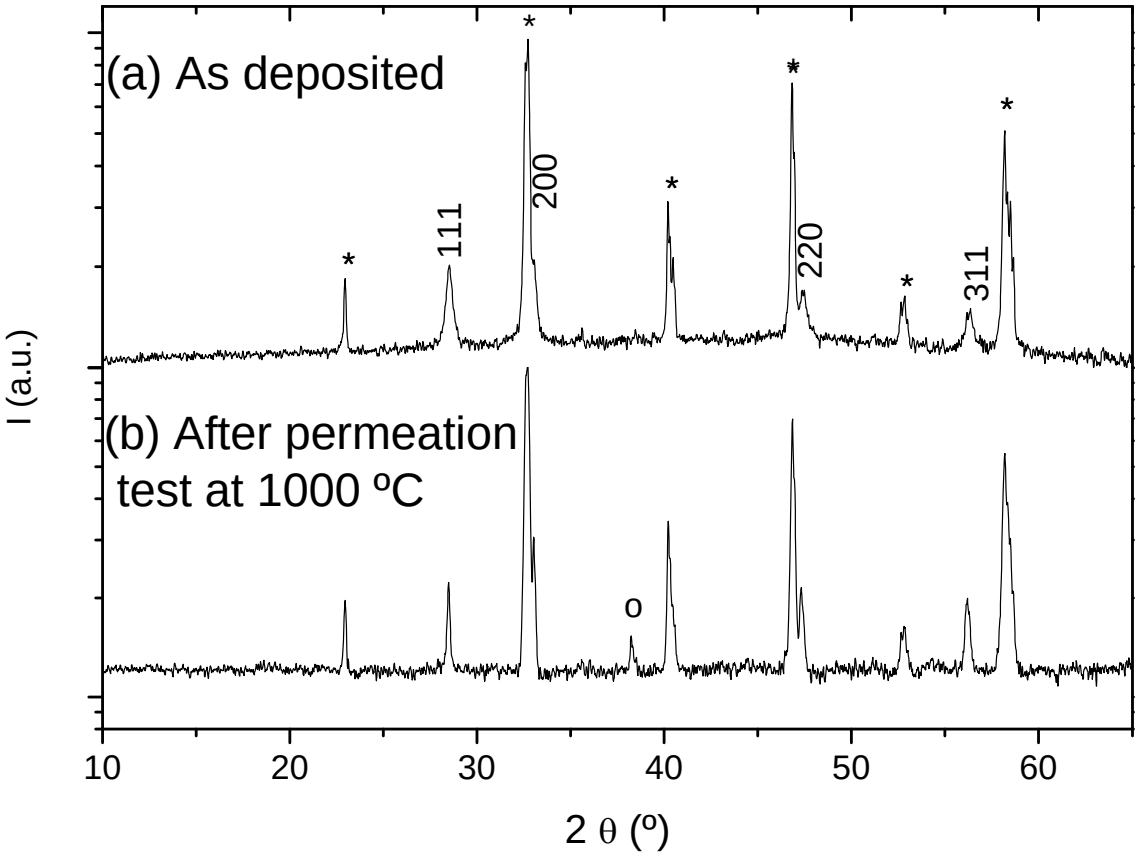
(a) As deposited
(b) After permeation test at 1000 ºC
111
200
220
311
*
o
I (a.u.)
2 θ (º)
10
20
30
40
50
60

Figure 6

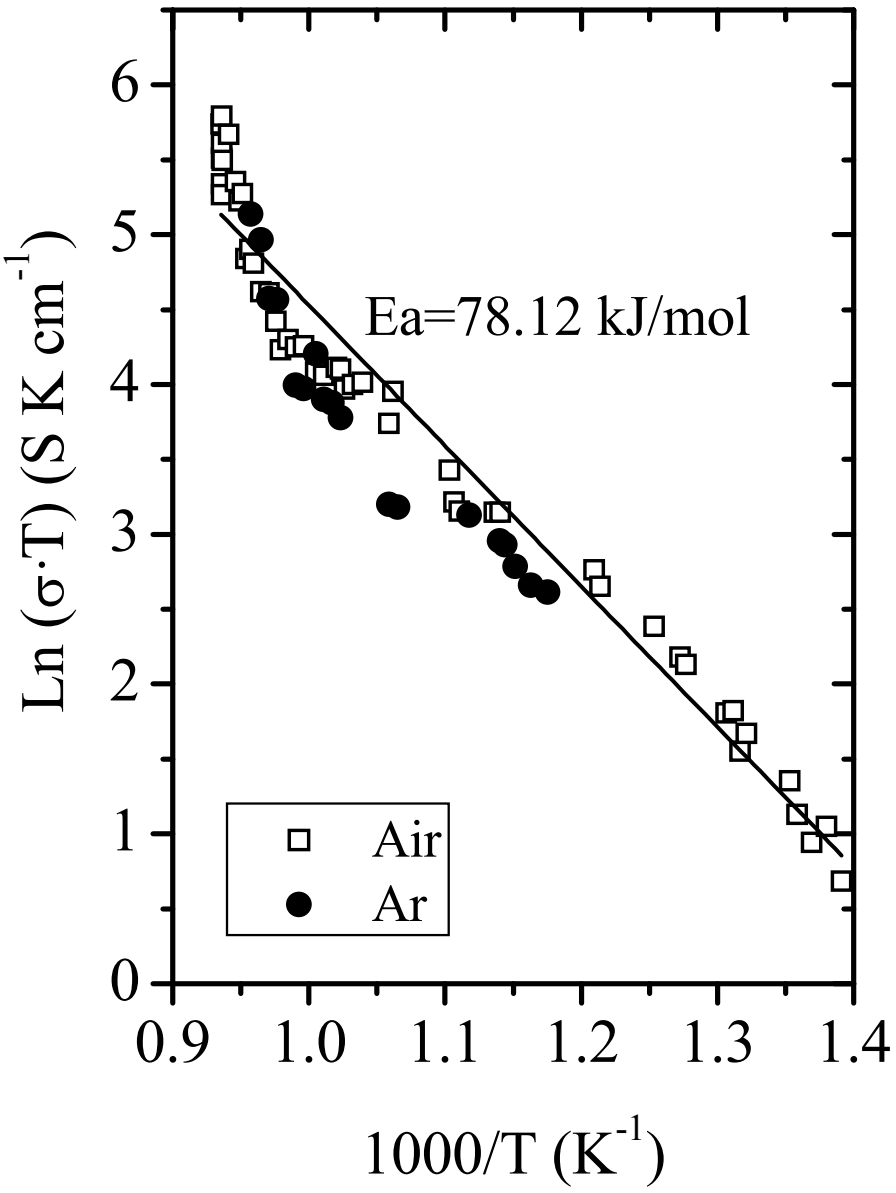
Ln (σ·T) (S K cm-1)
1000/T (K-1)
Ea=78.12 kJ/mol
Air
Ar
0
1
2
3
4
5
6
0.9
1.0
1.1
1.2
1.3
1.4

Figure 7

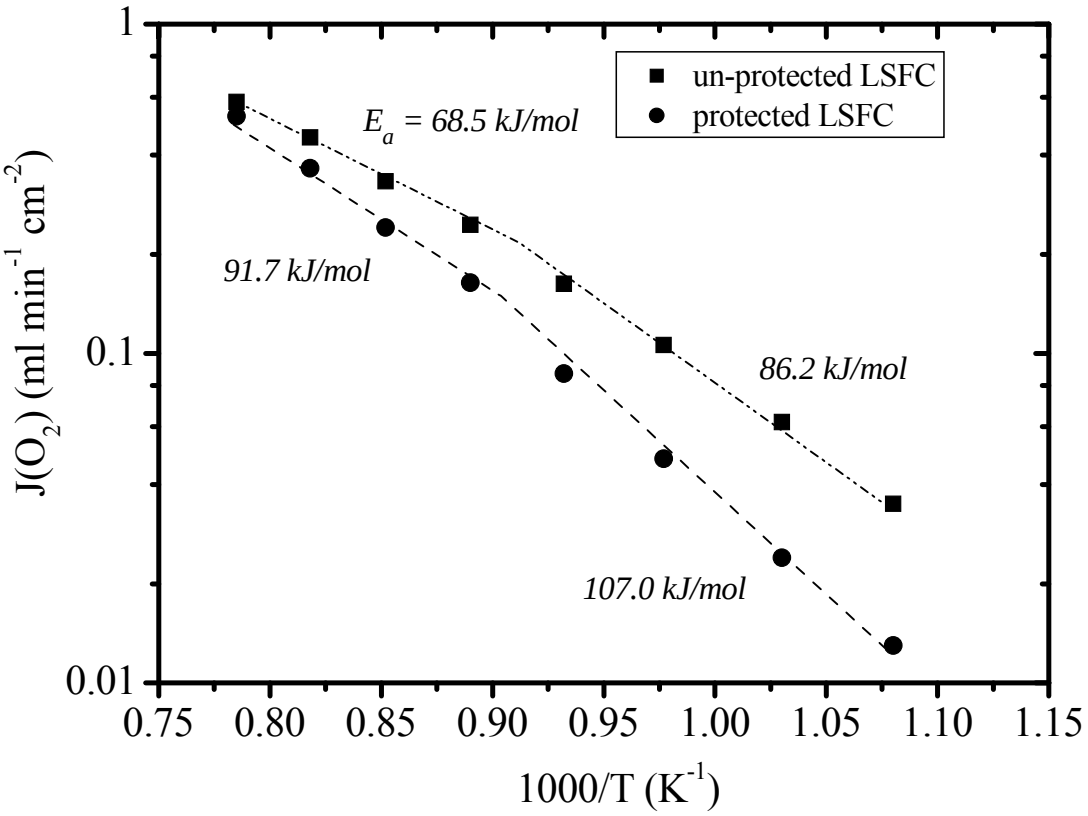
1
0.1
0.01
0.75
0.80
0.85
0.90
0.95
1.00
1.05
1.10
1.15
J(O2) (ml min-1 cm-2)
1000/T (K-1)
un-protected LSFC
protected LSFC
Ea = 68.5 kJ/mol
91.7 kJ/mol
86.2 kJ/mol
107.0 kJ/mol

Figure 8

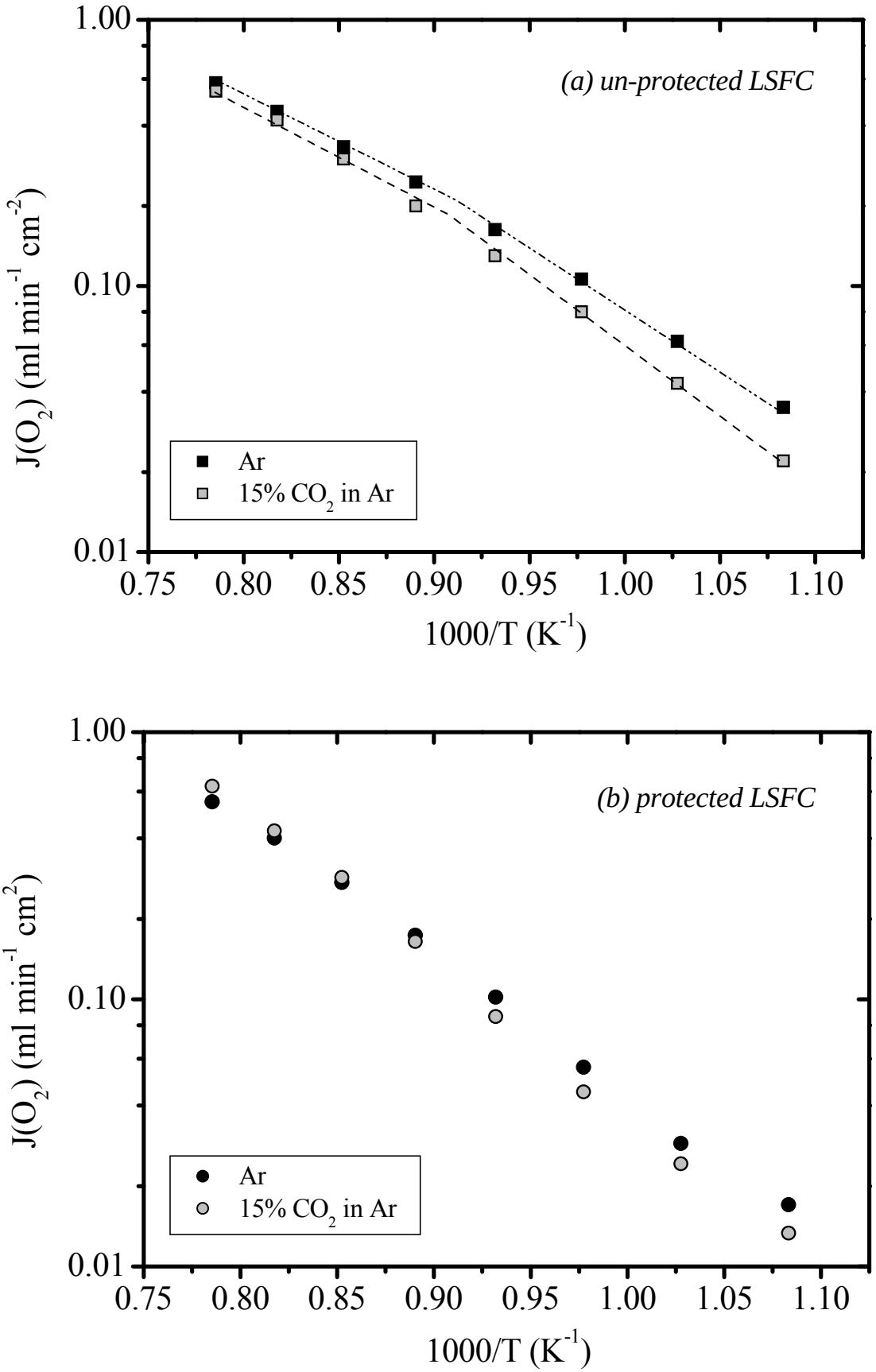
(a) un-protected LSFC
Ar
15% CO2 in Ar
J(O2) (ml min-1 cm-2)
1000/T (K-1)
1.00
0.10
0.01
0.75
0.80
0.85
0.90
0.95
1.00
1.05
1.10
(b) protected LSFC
Ar
15% CO2 in Ar
J(O2) (ml min-1 cm2)
1000/T (K-1)

Figure 9

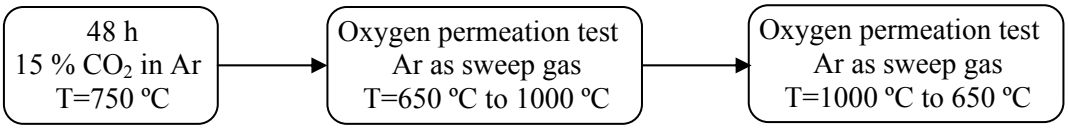
48 h
15 % CO_2 in Ar
T=750 ºC
Oxygen permeation test
Ar as sweep gas
T=650 ºC to 1000 ºC
Oxygen permeation test
Ar as sweep gas
T=1000 ºC to 650 ºC

Figure 10

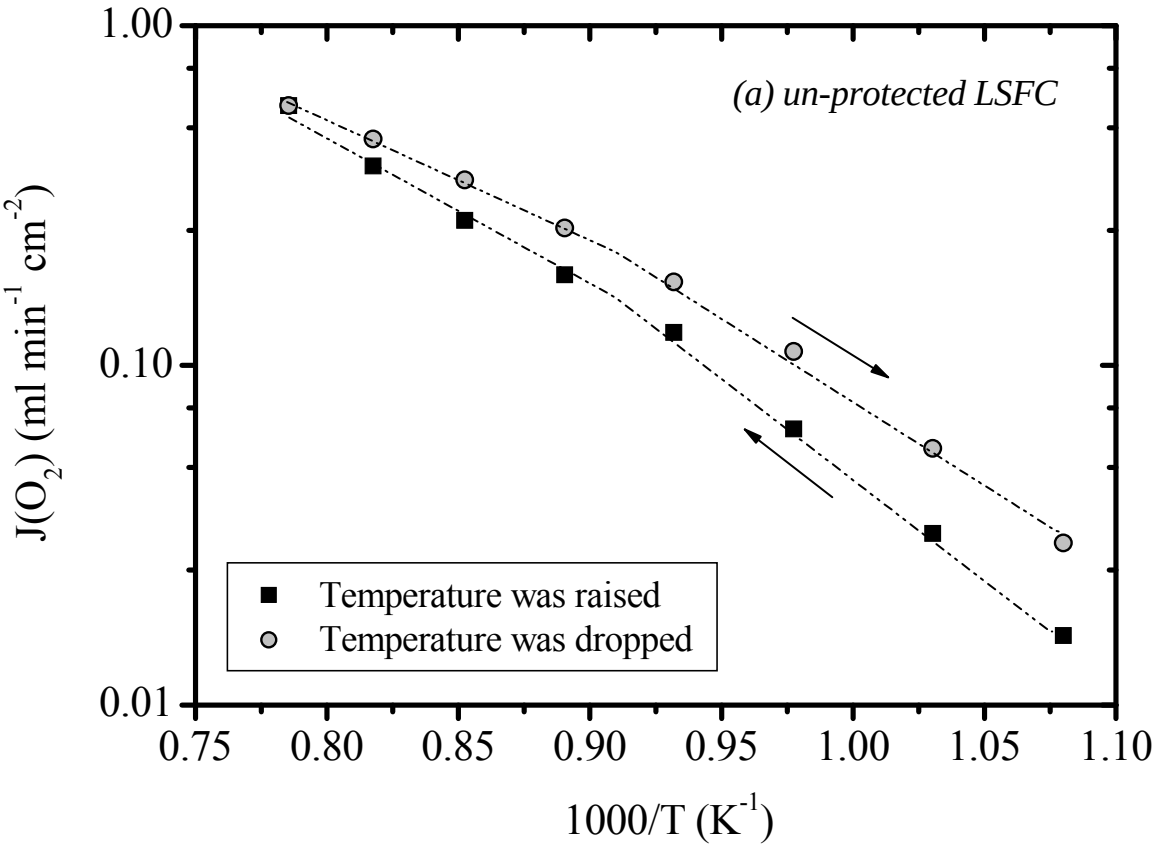
1.00
0.10
0.01
0.75
0.80
0.85
0.90
0.95
1.00
1.05
1.10
J(O2) (ml min-1 cm-2)
1000/T (K-1)
(a) un-protected LSFC
Temperature was raised
Temperature was dropped

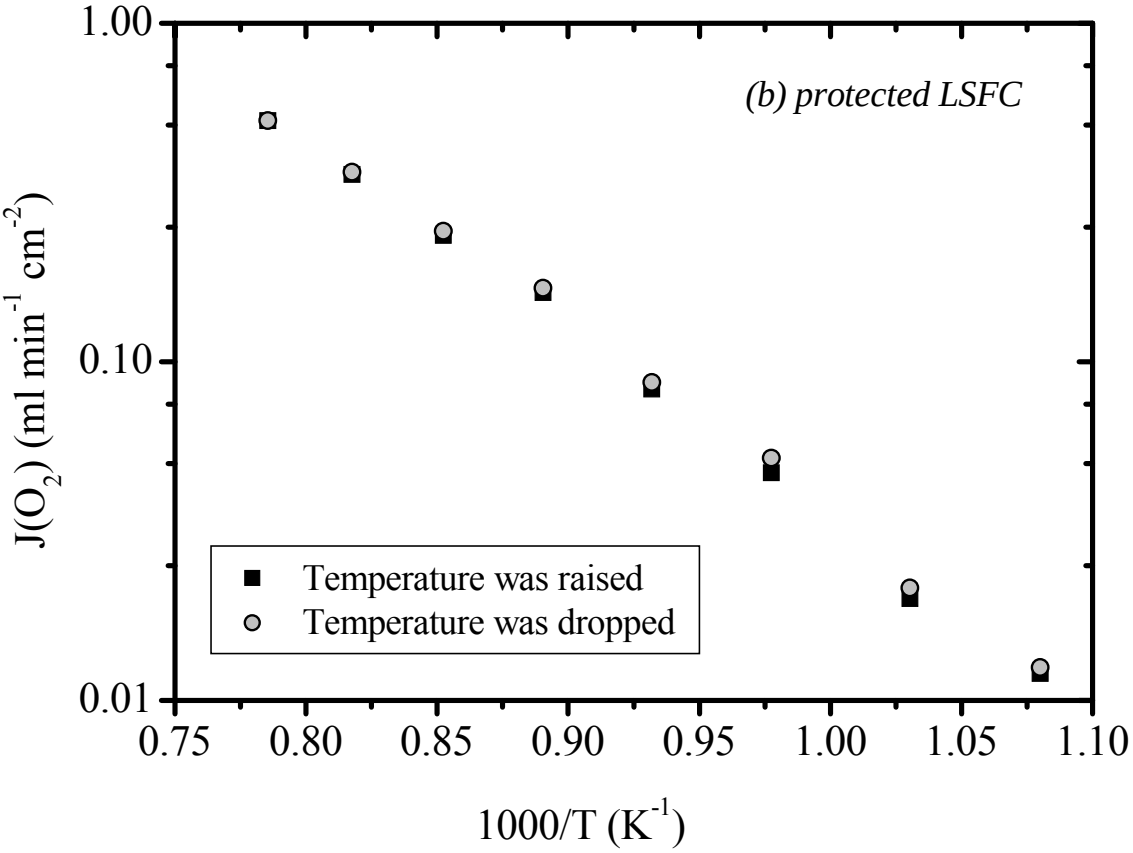
1.00
0.10
0.01
0.75
0.80
0.85
0.90
0.95
1.00
1.05
1.10
J(O2) (ml min-1 cm-2)
1000/T (K-1)
(b) protected LSFC
Temperature was raised
Temperature was dropped

Supporting Information

From “Development of CO_2 Protective Layers by Spray Pyrolysis for Ceramic Oxygen Transport Membranes” by Iván García, M. Pilar Lobera, Cecilia Solis, Pedro Atienzar, José M. Serra*

Figure S1

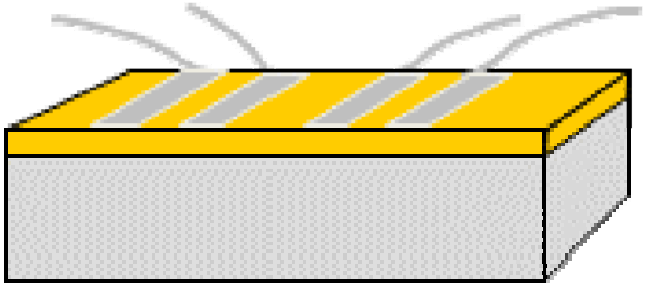

-.Configuration for the electrical measurements of the CGO layer on the sapphire substrate.-

Figure S2

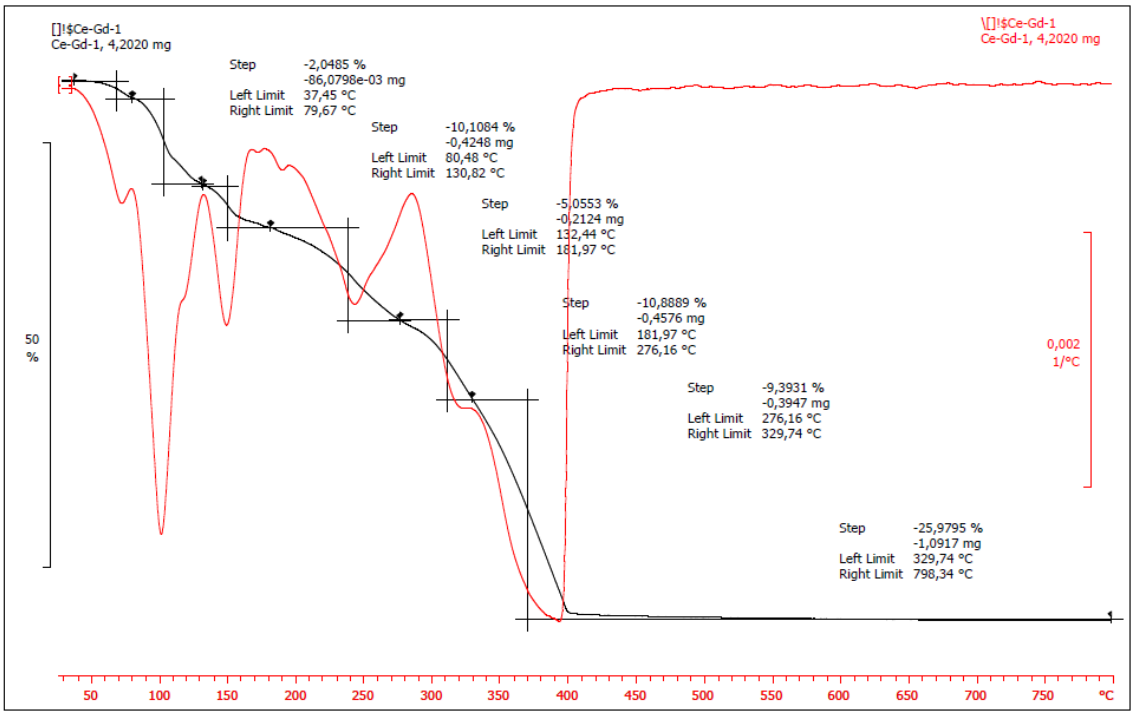

-.TGA measurement of CGO thin film precursor.-